Absorption Lines in the ISM

Absorption lines occur most often when cool gas lies between the observer and a hot source (typically a star or QSO), but can also result from a temperature gradient in an optically-thick medium.

The atoms (or ions) will generally be in a low-lying level such that absorption occurs from the ground state or levels close to the ground state. For hydrogen, almost all atoms are in n=1, so we only see Lyman series in absorption in interstellar matter. This may not be the case in optically thick, dense medium in stellar atmospheres.

A good reference is: B Savage and K Sembach *Ann. Rev. Astr. Astrophys. 1996. 34:279–329*
http://arjournals.annualreviews.org/doi/pdf/10.1146/annurev.astro.34.1.279

The equation of radiative transfer:

$$\frac{dI_\nu}{ds} = -\kappa_\nu I_\nu + \epsilon_\nu$$

where I_ν is the specific intensity, k_ν is the net absorption and ε_ν the volume emission coefficient

Line Absorption

The depth of the absorption is related to the column density of absorbing material (atoms in the lower level that produces the transition) and the absorption cross section. The line absorption coefficient *k* is given by:

$$k_{lu} = \int k_\nu \, d\nu = n_l \sigma_{lu}$$

Where the integral is over the line profile, and where the atomic absorption cross section $\sigma_{lu} = k_\nu / n_l$

The line absorption coefficient *k* has two components – the rate of absorption and the rate of stimulated emission

$$k_{lu} = \frac{h\nu_{ul}}{c}(n_l B_{lu} - n_u B_{ul})$$

$$k_{lu} = \frac{h\nu_{ul}}{c}(n_l B_{lu} - n_u B_{ul})$$

The Einstein B coefficients are related by

$$B_{ul} = \frac{g_l}{g_u} B_{lu}$$

And the A and B coefficients by:

$$B_{ul} = \frac{c^3}{8\pi h \nu_{ul}^3} A_{ul} \quad and \quad A_{ul} = \frac{8\pi^2 e^2 \nu^2}{m_e c^3} f_{ul}$$

where f_{ul} is the emission oscillator strength which is related to the absorption oscillator strength by the statistical weights:

$$g_u f_{ul} = g_l f_{lu}$$

In general, level populations are not in Thermal Equiibrium, so we use these relationships to estimate the 'departure coefficients' that reflect the variations in level populations. We have

$$\sigma_{lu} = \int_{line} \frac{k_\nu}{n_l} d\nu = \frac{h\nu_{ul}}{c}\left(B_{lu} - \frac{n_u}{n_l} B_{ul}\right) = \frac{h\nu_{ul}}{c} B_{lu}\left(1 - \frac{n_u g_l}{n_l g_u}\right)$$

$$\sigma_{lu} = \int_{line} \frac{k_\nu}{n_l} d\nu = \frac{h\nu_{ul}}{c}\left(B_{lu} - \frac{n_u}{n_l} B_{ul}\right) = \frac{h\nu_{ul}}{c} B_{lu}\left(1 - \frac{n_u g_l}{n_l g_u}\right)$$

A thermal population is given by:

$$\frac{n_u^*}{n_l^*} = \frac{g_u}{g_l} \; e^{-\Delta E_{ul}/kT_e}$$

The departure coefficients are $n_l = b_l n_l^*$ where n_l^* is the population given by a Boltzmann distribution so that the absorption cross section:

$$\sigma_{lu} = \sigma_{abs}\left(1 - \frac{b_u}{b_l} \; e^{-h\nu_{ul}/kT_e}\right)$$

defined in terms of an integrated atomic absorption cross section σ_{abs}

$$\sigma_{abs} = \frac{h\nu_{ul}}{c} B_{lu} = \frac{\pi e^2}{m_e c} f_{lu}$$

Absorption lines with hν >> kT$_e$

$$\sigma_{lu} = \sigma_{abs}\left(1 - \frac{b_u}{b_l}\; e^{-h\nu_{ul}/kT_e}\right)$$

Absorption lines in the optical and UV have hν >> kT$_e$. The exponential term become small, so that stimulated emission becomes negligible and we can treat this as pure absorption.

In the ISM almost all species are in the ground state, so we can say that $\sigma_{lu} = \sigma_{abs}$

Oscillator strengths are listed e.g. in Astrophysical Quantities (by C W Allen) or in the NIST databse.

Absorption Lines with hν << kT$_e$

At long wavelengths, where hν << kT$_e$, the exponential term tends to unity, and we can expand the exponential term to give

$$\sigma_{lu} \approx \sigma_{abs}\left(1 - \frac{b_u}{b_l}\left(1 - \frac{h\nu_{ul}}{kT_e}\right)\right)$$

In LTE, $b_u = b_l = 1$ so this becomes:

$$\sigma_{lu} = \sigma_{abs}\left(\frac{h\nu_{ul}}{kT_e}\right)$$

i.e. the pure absorption cross section is reduced by a factor hν/kT$_e$ by stimulated emission

Non-LTE Absorption Lines with hν << kT$_e$

$$\sigma_{lu} = \sigma_{abs}\left(1 - \frac{b_u}{b_l}\left(1 - \frac{h\nu_{ul}}{kT_e}\right)\right)$$

In extreme non- LTE, the population in the upper level can exceed that in the lower level, in which case b_u/b_l can become >1 and > (1- hν/kT$_e$) leading to the expression becoming negative and the emissive component exceeding the absorption.

This occurs in masers, which are found in the microwave and radio regions, mostly in diatomic molecules such as OH and SiO but also in methanol and HCN. The population inversions can lead to enormous brightness temperatures.

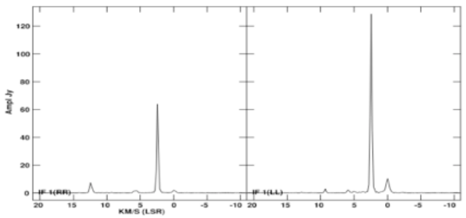

(f) W75 N 1665 MHz

UV and Optical absorption lines

In the Interstellar Medium, background stars reveal narrow but resolved absorption from neutral atoms or singly ionized species (with low I.P.)

A list from ~ 10 years ago measured in the UV with the Goddard High Resolution Spectrograph on the HST is given here, but note that many more species have been measured with other instruments, and at other wavelengths.

The measurements are used to investigate the abundances, kinematics and physical conditions in the ISM. Note that geocoronal Lyman alpha makes it difficult to measure Lyα at its rest wavelength, but observations of redshifted Lyα are extremely important for understanding the intergalactic medium at high redshift

Atoms[a] (1150 < λ < 3200 Å)	Z[b]	IP(eV)[c] (I to II)	IP(eV)[c] (II to III)	$\log(X/H)_m + 12$[d]
H I	1	13.60	…	12.00
D I	1	13.60	…	….
B II	5	8.30	25.15	2.88±0.04
C I, C I*, C I**, C II, C II*, C IV	6	11.26	24.38	8.55±0.05
N I, N V	7	14.53	29.60	7.97±0.07
O I, O I*	8	13.62	35.12	8.87±0.07
Mg I, Mg II	12	7.65	15.04	7.58±0.02
Al II, Al III	13	5.99	18.83	6.48±0.02
Si I, Si II, Si II*, Si III, Si IV	14	8.15	16.35	7.55±0.02
P I, P II, P III	15	10.49	19.73	5.57±0.04
S I, S II, S III	16	10.36	23.33	7.27±0.05
Cl I	17	12.97	23.81	5.27±0.06
Cr II	24	6.77	16.50	5.68±0.03
Mn II	25	7.44	15.64	5.53±0.04
Fe II	26	7.87	16.18	7.51±0.01
Co II	27	7.86	17.06	4.91±0.03
Ni II	28	7.64	18.17	6.25±0.02
Cu II	29	7.73	20.29	4.27±0.05
Zn II	30	9.39	17.96	4.65±0.02
Ga II	31	6.00	20.51	3.13±0.03
Ge II	32	7.90	15.93	3.63±0.04
As II	33	9.81	18.63	2.37±0.05
Se II	34	9.75	21.19	3.35±0.03
Kr I	36	14.00	24.36	3.23±0.07
Sn II	50	7.34	14.63	2.14±0.04
Tl II	81	6.11	20.43	0.82±0.04
Pb II	82	7.42	15.03	2.05±0.03

Molecules: $H_2(v = 3)$, OH, ^{12}CO, ^{13}CO, $C^{17}O$, $C^{18}O$, C_2, HCl

Equivalent Width

The amount of light absorbed in a spectral line is often expressed in terms of the *equivalent width*. This quantity is the width (in wavelength units) that the line would have if it were completely black.

It has the very useful feature that the amount of absorption is normalised to the continuum and so does not rely on an accurate flux calibration.

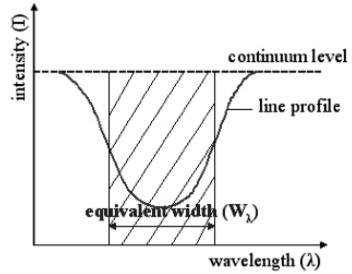

$$EW = \int \frac{F_{cont} - F_{line}}{F_{cont}} d\lambda = \frac{\lambda_0}{\nu_0} \int (1 - \frac{I_\nu}{I_{\nu_0}}) d\nu = \frac{\lambda_0}{\nu_0} \int (1 - e^{-\tau_\nu}) d\nu$$

The biggest uncertainty is often in placing the continuum

Column Density from optically thin lines

The optical depth depends on the oscillator strength and the column of atoms so that

$$\frac{\lambda}{\upsilon}\tau = \frac{\pi e^2}{m_e c^2} f \lambda^2 N_l = EW$$

or for the optically thin case (weak absorption) with $\tau << 1$

$$N(cm^{-2}) = 1.13 \times 10^{17} \frac{W_\lambda(m\overset{o}{A})}{f\lambda^2(\overset{o}{A})}$$

If we have two optically thin lines originating from a split lower level, we can use the Boltzmann formula to estimate excitation temperature from:

$$\frac{W_{\lambda 2}}{W_{\lambda 1}} = \frac{f_2 \lambda_2^2}{f_1 \lambda_1^2} \frac{g_2}{g_1} e^{-(\Delta E / kT)}$$

Neutral Carbon

Configuration	Term	J	Level (cm^{-1})
$2s^2 2p^2$	^3P	0	0
		1	16.40
		2	43.40
$2s^2 2p^2$	^1D	2	10 192.63
$2s^2 2p^2$	^1S	0	21 648.01
$2s2p^3$	$^5S°$	2	33 735.20
$2s^2 2p(^2P°)3s$	$^3P°$	0	60 333.43
		1	60 352.63
		2	60 393.14
$2s^2 2p(^2P°)3s$	$^1P°$	1	61 981.82
$2s2p^3$	$^3D°$	3	64 086.92
		1	64 089.85
		2	64 090.95

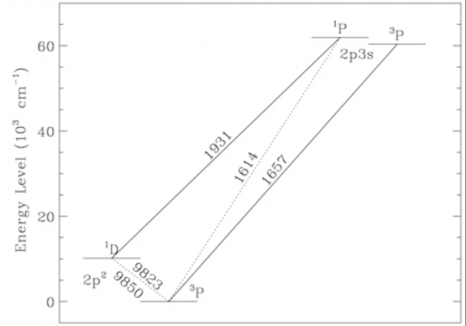

C I has a split ground state and 1[st] excited state at ~60350 cm^{-1} giving transitions at ~1657 Å.

	λ (Å)	f
$2s^2 2p(^2P)3s\ ^3P_0 - 2s^2 2p^2\ ^3P_1$	1657.91	0.048
$2s^2 2p(^2P)3s\ ^3P_1 - 2s^2 2p^2\ ^3P_0$	1656.93	0.143
$2s^2 2p(^2P)3s\ ^3P_1 - 2s^2 2p^2\ ^3P_1$	1657.38	0.036
$2s^2 2p(^2P)3s\ ^3P_1 - 2s^2 2p^2\ ^3P_2$	1658.12	0.036
$2s^2 2p(^2P)3s\ ^3P_2 - 2s^2 2p^2\ ^3P_1$	1656.27	0.059
$2s^2 2p(^2P)3s\ ^3P_2 - 2s^2 2p^2\ ^3P_2$	1657.01	0.101

electric dipole selection rules $\Delta J = 0, \pm 1, \neq 0-0$

CI absorption at high z

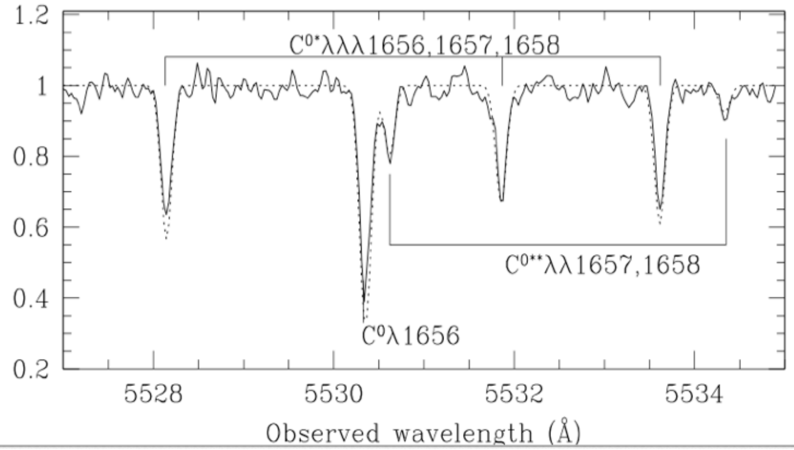

High resolution spectroscopy by Srianand et al (2001) towards a QSO, PKS 1232+0815, z =2.338

C^0 refers to absorption from $^3P_0$, C^{0*} from $^3P_1$ and C^{0**} from $^3P_2$

From these measurements, the excitation temperature can be estimated from the EW :

$$\frac{W_{\lambda 2}}{W_{\lambda 1}} = \frac{f_2 \lambda_2^2}{f_1 \lambda_1^2} \frac{g_2}{g_1} e^{-(\Delta E / kT)}$$

The excitation can arise from e^- or atomic collisions or photons. C I arises from neutral regions so H atom collisions may dominate over electron collisions.

The ground state splitting of 16.4 and 27 cm^{-1} produces IR lines at 609 and 374 µm, which can be used as a thermometer for the radiation temperature. (They were major targets for the Herschel satellite)

Cosmological models indicate that $T_{CMB} = T_0(1+z)$, and so at z~2.3, we expect T to increase from 2.73 K now to 9 K then, giving a marked increase in the population in the $^3P_1$ / $^3P_0$ ratio.

Table 1. Excitation rates $K_{JJ'}$ of the C^0, C^+ and O^0 fine-structure levels by the CMBR. We have assumed the temperature–redshift relation as predicted by the standard model (see text).

	C^0		C^+	O^0
z	K_{01} (s^{-1})	K_{02} (s^{-1})	$K_{\frac{1}{2}\frac{3}{2}}$ (s^{-1})	K_{21} (s^{-1})
0	4.2×10^{-11}	1.2×10^{-23}	1.4×10^{-20}	3.0×10^{-41}
1	3.2×10^{-9}	1.1×10^{-18}	2.5×10^{-13}	4.0×10^{-23}
2	1.4×10^{-8}	5.0×10^{-17}	6.6×10^{-11}	4.4×10^{-17}
3	3.1×10^{-8}	3.4×10^{-16}	1.1×10^{-9}	4.6×10^{-14}
4	5.1×10^{-8}	1.1×10^{-15}	5.7×10^{-9}	3.0×10^{-12}
5	7.4×10^{-8}	2.3×10^{-15}	1.7×10^{-8}	4.8×10^{-11}

Model calculations (Silva & Viegas 2002) for the changing excitation rates with $T_{CMB} = T_0(1+z)$ [where $K_{ij} = B_{ij} u_{ij}$]
The values for PKS 1232 are consistent with increased T_{CMB}

Herschel SPIRE Spectrum of the Helix nebula

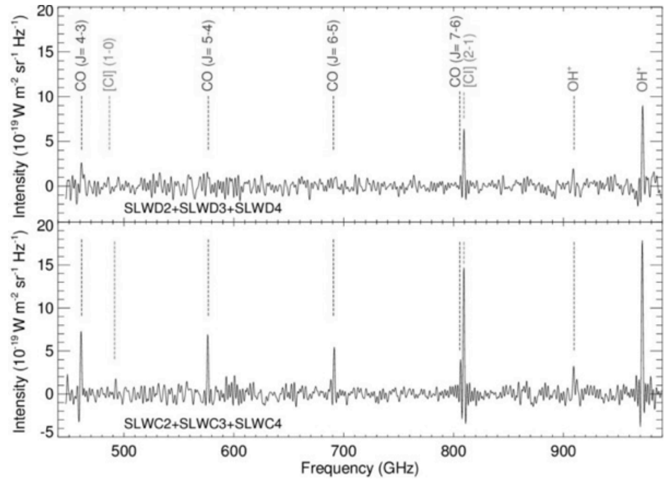

This nearby planetary nebula show the 609 and 374 µm CI lines together with excited CO molecular rotational lines. The spectra at two positions in the nebula are shown.

Historical Digression:

In 1941, Andrew McKellar found that from measurements of the CN molecule the 'rotational temperature' of interstellar space is about ~2 K, later refining this to 2.3 K.

This predated the discovery of the CMB by >20 years, but the significance was not realised at the time.

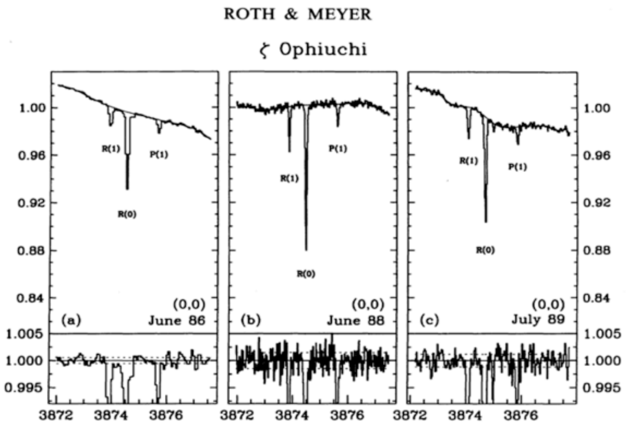

The Curve of Growth

In the optically thick case, the absorption in the centre of the line saturates, and the equivalent width grows slowly as the wings of the profile extend away from the core, following the 'curve of growth'.

Initially the line depth increases with $W_\lambda \propto N$ linearly, but when the core saturates, the doppler wings increase very slowly and $W_\lambda \propto \sqrt{Ln(N)}$ until the collisional broadening wings dominate and $W_\lambda \propto \sqrt{N}$

It is difficult to make reliable estimates of N in the middle regime as W_λ depends on N/b, where b is the broadening.

The plot shows a gaussian profile for τ= 0.06, 0.12,0.25…4, 8

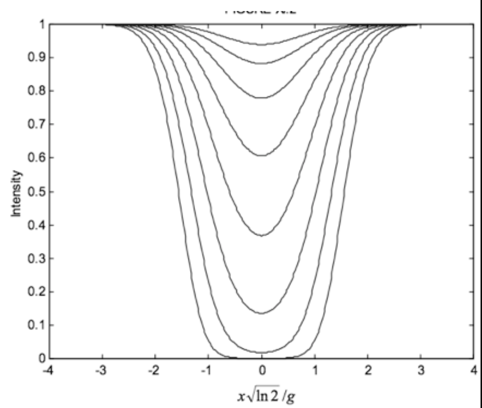

Curve of Growth

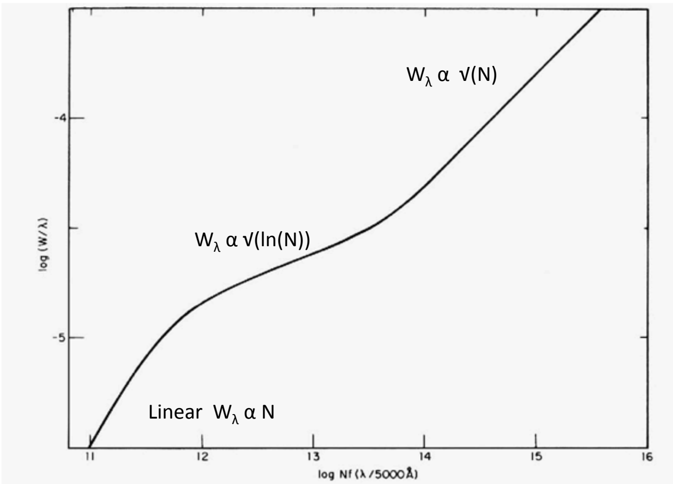

Curve of growth from Aller (1944)

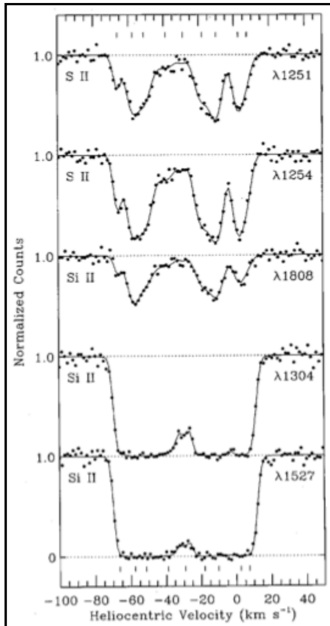

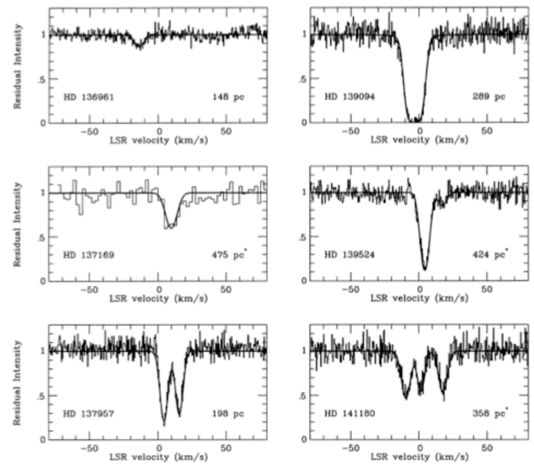

Figure 2. The interstellar Na D_2 lines towards the observed stars. The observed data are plotted as histograms, and the theoretical line profiles with the parameters given in Table 1 are shown superimposed. Distances are from *Hipparcos*, unless marked *, in which case they are less certain photometric values

Interstellar lines measured in the UV/optical.

We can get relative abundances and conditions from different kinematic components (clouds along the line of sight)

At high resolution, the line profiles can be measured to investigate broadening mechanisms. Heavier species will show narrower profiles for thermal broadening.

Generally expressed in terms of a velocity dispersion parameter, b

$$b = \sqrt{\frac{kT_k}{m} + 2v_t^2}$$

where v_t is the line of sight turbulent velocity

Calculations of columns for different elements allow assessment of element abundances in the gas phase.

Deviations from cosmic abundance imply depletion of refractory elements into dust grains

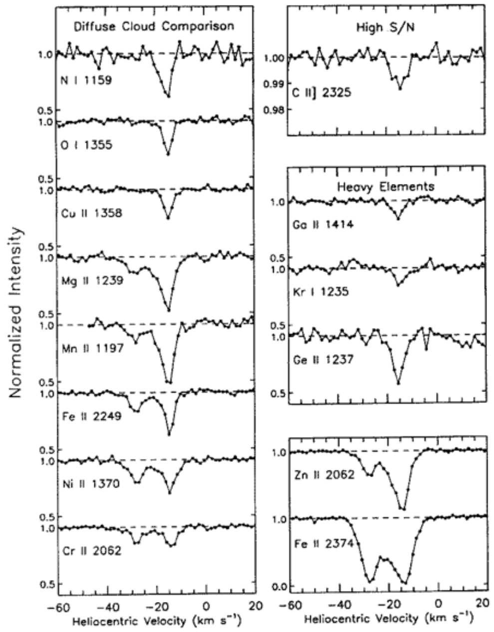

Observations of many stars in a region can map out different components, or time series spectroscopy over years may reveal change in circumstellar or interstellar columns.

These observations show the component at 22km/s varied towards δ Ori over 6 years and could be due to ionization or density variations. The spectra, taken at the AAT) have R~ 900,000.

(from Crawford 2003)

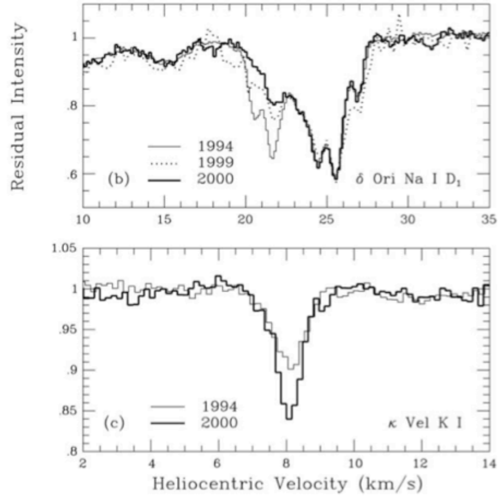

Depletions

- High resolution spectroscopy from the ground and satellites provides columns of different elements and ions in the gas phase:
  - 'missing' species compared to adopted cosmic abundance are presumed to have condensed into dust where the narrow atomic transitions are suppressed.
  - Degree of depletion correlates with condensation temperature
  - Places severe constraints on the composition of interstellar dust
  - Dominated by O, C, Si, Mg, Fe, Ca

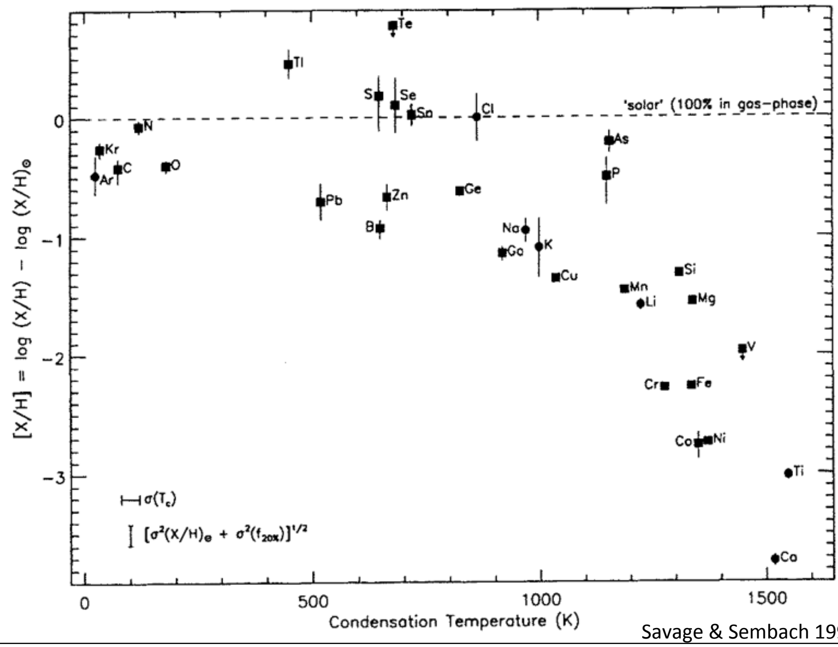

Savage & Sembach 1996

The Lyman alpha forest

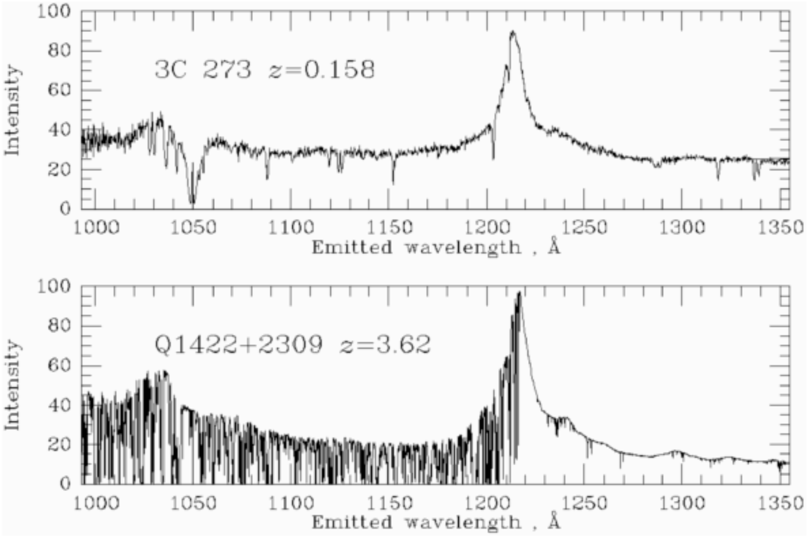

Deuterium Abundance towards QSO
SDSS J155810-003120 (O'Meara et al 2006)

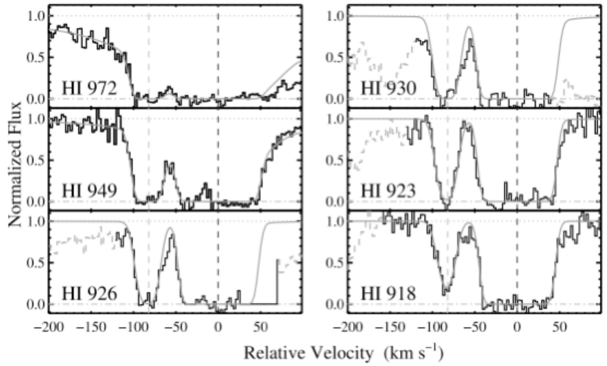

The Hydrogen – Deuterium isotopic shift is 82km/s. The H lines are heavily saturated with pronounced damping wings. Deuterium becomes optically thin by Ly 11 (918Å), with a line width ~10km/s, but we have to rely on the curve of growth to model H column and estimate D/H.

Deuterium Abundance

Oscillator strengths for D are the same as H, so columns are given directly by the line depths.

The average value of D/H towards 6 high-z QSOs (with IGM metallicity ~1/30 solar) is $2.5.10^{-5}$, compared to the value in the local Galactic ISM of $1.56.10^{-5}$.

But, variations both within the Galaxy and amongst IGM sightlines are greater than errors indicate suggesting real scatter in D/H.

Variations with redshift may be due to Astration, but isotopic fractionation may also be important.

D/H of $2.5.10^{-5}$ gives Ω_B fraction = 0.044, consistent with WMAP Big Bang models

QSOs from

5.7 <z < 6.4 showing the increasing absorption depth (Fan et al 2006) and the onset of significant neutral H (Gunn Peterson Trough)

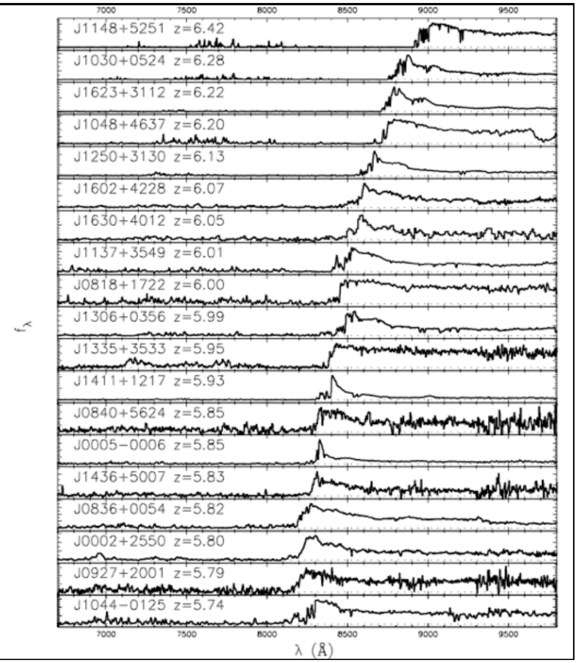

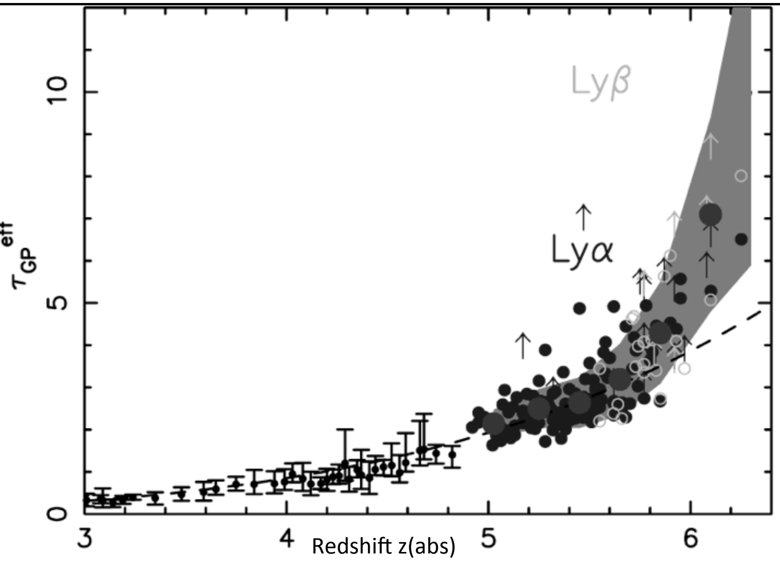

The Hydrogen optical depth appears to increase rapidly beyond z = 6. The dashed line represents Tau(GP) ~$(1+z)^{4.3}$: the increase beyond z~5.8 suggests that the neutral fraction increases rapidly. (from Fan 212)

Evolution of the mean free path of ionizing photons

Results inferred from observations (Fan 2006) compared with the simulations of Gnedin (2004)

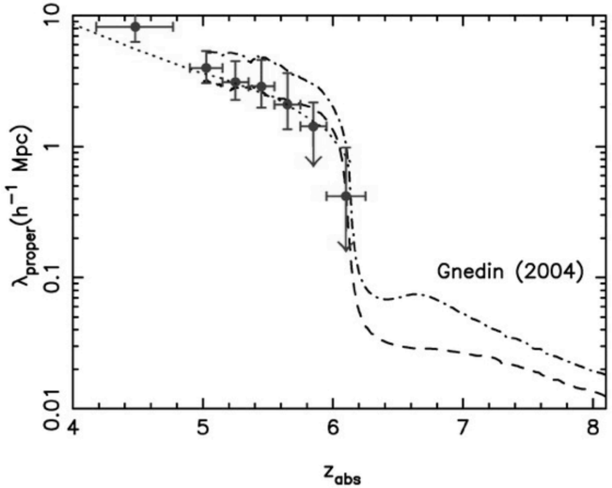

Normalised spectra of high-z QSOs from Bolton et al 2012, plotted against velocity centred on rest- frame Lya Red lines are the estimated intrisic flux levels continuum and Lya emission lines.

These spectra are used to investigate the physical conditions in the IGM around the QSOs.

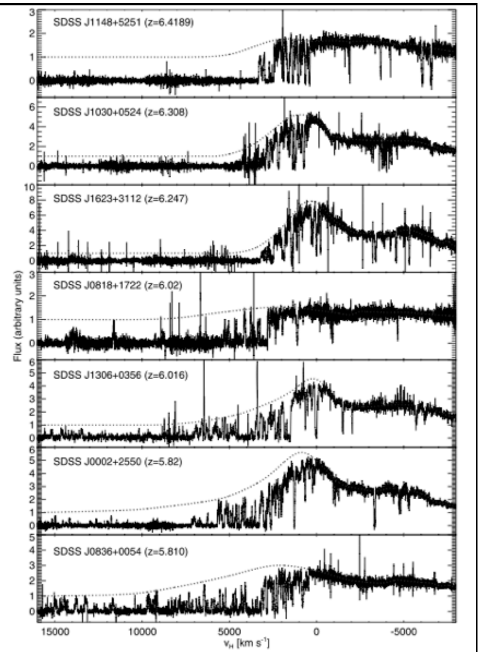

Absorption line studies

High resolution spectra allow detailed investigation of absorption components of the interstellar medium within the Milky Way and the intergalactic medium to z~ 7.

High precision measurements of quasar absorption lines have also been used to test the universality of the laws of physics e.g. by searching for variations in the fine structure constant, α, and the proton-electron mass ratio, μ.

So far, limits of a few ppm (e.g. Bonifacio et al 2014) have been set, but claims of small variations in different directions on the sky have been made (e.g. King et al 2012).

Extremely stable, high resolution spectrographs on the Extremely Large Telescope may be able to measure the changes in the rate of expansion of the Universe directly with observations over a few decades..

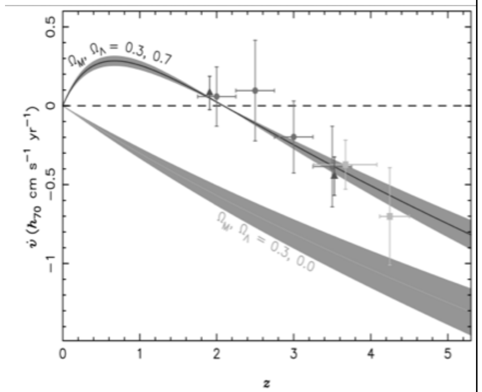

Fig. 1 The *solid lines* show the redshift drift as a function of redshift in velocity units for two different combinations of Ω_M and Ω_Λ as indicated, and a Hubble constant of $H_0 = 70$ km s^{-1} Mpc^{-1}. The *grey shaded areas* result from varying H_0 by ±8 km s^{-1} Mpc^{-1}. The three sets of 'data' points show Monte Carlo simulations of a redshift drift experiment with CODEX/E-ELT using a total of 4000 h observing time and a total experiment duration of 20 yr.

Liske et al 2008